

# Effect of Microstructure and Properties of Ni-WC Composite Coatings on Their Solid Particle Erosion Behavior

Sima A. Alidokht, Jacques Lengaigne, Jolanta E. Klemberg-Sapieha, Steve Yue, and Richard R. Chromik

(Submitted September 17, 2018; in revised form December 19, 2018; published online February 28, 2019)

Metal matrix composites (MMCs) of WC in Co or Ni matrices are widely used due to their high wear resistance. Previous studies showed that tailoring the mechanical properties through optimum WC content can significantly extend the life cycle of MMCs. In this study, composite coatings of Ni with various WC content ranging from 10 to 55 vol.% were cold sprayed using agglomerated WCNi powders and two different sizes of Ni powders, – 10 + 4 ( $d_{50} = 7 \mu\text{m}$ ) referred to as Ni(7) and – 35 + 15 ( $d_{50} = 25 \mu\text{m}$ ) to as Ni(25). Microstructural characterization, including the deformed structure of Ni splats and retention and distribution of WC, was performed by scanning electron microscopy (SEM). Composite coatings were subjected to solid particle erosion following ASTM G76-13 standard. At low WC content coatings, erosion occurred primarily by plastic deformation of Ni matrices and knocking out of WC particles. At high WC concentrations, network distribution of compacted WCNi particles in the matrices led to a significant drop in erosion rates of coatings, due to a change in erosion mechanism from severe cutting and plowing of Ni and WC dislodging to WCNi splats spalling. Composite coatings sprayed using finer size Ni powder were usually more erosion resistant.

**Keywords** cold spray, mean free path, metal matrix composite, solid particle erosion, subsurface microstructure, WC

## 1. Introduction

Solid particle erosion (SPE) is the wear of materials that occurs when hard solid particles are entrained in a fluid and impinge on a surface. SPE is involved with a series of independent but similar impact events where erodent particles hit the surface (Ref 1, 2). In SPE, the materials are traditionally divided into ductile and brittle based on their response to wear. Ductile materials often exhibit maximum erosion rates at small impact angle, while for brittle materials, a high erosion damage is detected at normal angle of incidence (Ref 3, 4). Recently much attention has been paid to metal matrix composite (MMC) coatings which combine hardness of hard ceramic particles with toughness of metallic binder to control and minimize erosion damage for a wide range of impact angles (Ref 5, 6). Refractory carbides such as WC, TiC, and  $\text{Cr}_2\text{C}_3$  particles are commonly used for prolonged protection of surfaces against erosion damage (Ref 7-9).

The wear resistance of WC-reinforced MMC coatings has been studied previously. Ramesh et al. (Ref 10) investigated

SPE of HVOF-deposited NiCrFeSiB and 35 vol.% WC-Co/NiCrFeSiB coatings. They showed that plowing and cutting of the Ni matrix and dislodging of WC fragments are the prevailing erosion mechanisms at low angle of attack, whereas crater formation and spalling of the coating following subsurface cracking were indicative of a composite ductile and brittle mode at 90° attack angle. Higher erosion rate was recorded for composite coating when compared to that of uncoated steel. Embedding of SiC erodent particles into relatively softer uncoated steel was found to impart shielding effects against impinging particles leading to lower erosion loss. Studies of Kulu and co-workers (Ref 7, 9) showed that the erosion wear resistance of reference materials like uncoated steel or Ni coatings can be greatly improved by incorporation of a sufficiently high WC-Co content, above 70 vol.% WC content, into the metallic matrices. Paul et al. (Ref 8) conducted SPE testing using  $\text{Al}_2\text{O}_3$  erodent particles on high content Ni-WC laser clad surfaces with 75-92 vol.% WC. Worn surface observation revealed that ductile erosion mechanisms followed by the removal of WC particulates from the matrix dominate the erosion damage. They found that erosion behavior of composite coatings was primarily governed by erodent particles velocity followed by their impact angle. Gee et al. (Ref 11) and Hussainova et al. (Ref 12) performed SPE on WC-12Co hard metals, accumulation of plastic strain in WC, intergranular cracking, interphase debonding, and microcracking of carbides.

In another study, Zhou et al. (Ref 13) observed that the coatings of 35 vol.% cast WC-reinforced iron matrix showed the highest erosion resistance under impact angle of 70°. They observed the worn surfaces with a characteristic protruding of WC particles and sinking of the matrix, indicating preferential wear of matrices and a high resistance of WC particles against erosion damage, due to their significantly higher hardness compared to the silica erodent particles. With increasing WC content up to 35 vol.%, erosion rates were reduced. However,

**Sima A. Alidokht, Steve Yue, and Richard R. Chromik**, Department of Mining and Materials Engineering, McGill University, M.H. Wong Building, 3610 University Street, Montreal, QC H3A 0C5, Canada; and **Jacques Lengaigne and Jolanta E. Klemberg-Sapieha**, Department of Engineering Physics, Polytechnique Montréal, P.O. Box 6079, Station Centre-ville, Montréal, QC H3C 3A7, Canada. Contact e-mail: richard.chromik@mcgill.ca.

further increase in WC content above 35 vol.% led to rise in erosion of the composites. The increase in erosion rates of composites for volume fraction above 35 vol.% was linked to weak interfacial bonding at high WC contents, where the matrix between WC became too little or nonexistent, leading to WC particles contacting each other. The result is an increase in erosion damage, since the supporting effect of the matrix to WC particles through a good interface bond is essential for the protecting effect of WC particles (Ref 13). This emphasizes the importance of matrix mechanical properties and erosion resistance, as well as, microstructural factors, i.e., spacing between reinforcement particles, their size, and volume fractions. However, the relationship between microstructure, matrix and hard particles, and wear parameters is critical as well.

Due to its distinct advantages over traditional thermal spray processes, cold spray has been developed to deposit WC-containing composites over the last decade. Cold spray is a solid-state process, in which oxidation, decomposition, and any other unwanted phase transformation of heat-sensitive feedstock such as WC particles can be avoided (Ref 14-19). While many examples of WC-based MMCs by cold spray exist in the literature (Ref 16, 17, 20-23), very few have studied the erosion performance in detail (Ref 20, 21). Erosion performance of cold-sprayed WC-CoCr, Cr<sub>3</sub>C<sub>2</sub>-NiCr, and Al-Al<sub>2</sub>O<sub>3</sub> coatings was tested in a previous study (Ref 24). Friction stir processing (FSP) was used to improve the distribution of reinforcing particles within the matrix. Reduction in the interparticle spacing led to less of the matrix alloy being exposed to the impinging particles, and hence, erosion resistance was improved. The SPE of cold-sprayed Ni and Ni-10.5 vol.% cast WC was studied previously by the authors (Ref 25). For impact angles of 30° and 90°, worn morphologies associated with ductile erosion including cutting, plowing, lips formation, and its embrittlement was observed on the Ni matrices. At low impact angle, WC particles were least damaged due to erosion but were knocked out when the supporting effect of Ni matrix was reduced due to matrix erosion. Under normal angle, eroded surfaces showed brittle cracking of WC particles and fragmentation and following removal from the surface. The addition of a 10.5 vol.% cast WC did not significantly improve the erosion resistance at low impact angle (Ref 25). Higher WC content likely would improve erosion properties, but this was not possible using cast WC particles (Ref 25). Other studies showed that by using agglomerated WC-Co or WC-Ni particles, higher WC content can be achieved that is closer to that of initial feedstock (Ref 17-19). SPE performance of cold-sprayed Ni-WC with various WC content has not been conducted yet and was therefore the main focus of the current study. Moreover, the influence of Ni matrix microstructure and hardness on SPE was tested using two size range Ni powders, referred to as Ni(7) and Ni(25). In a previous work by the authors (Ref 19), coatings of pure Ni(7) and Ni(7)-WCNi were cold sprayed and mechanisms of WCNi retention and Ni-deformed microstructure evolution were discussed. The present study is largely limited to a discussion of powder size effect on Ni coatings microstructure, as well as, SPE mechanisms of Ni and composite coatings.

## 2. Experimental

### 2.1 Cold-Sprayed Coatings Characterization

Feedstock powders for cold spray were commercially pure gas-atomized Ni (AMPERIT® 176, HC Starck, Germany)

referred to as Ni(25), commercially pure water-atomized Ni (4SP-10, Novamet, USA) referred to as Ni(7), and agglomerated and sintered WCNi (AMPERIT® 547, HC Starck, Germany) (Fig. 1). The Ni(7), Ni(25), and WCNi powders had particle size ranges of  $-10 + 4$  ( $d_{50} = 7 \mu\text{m}$ ),  $-35 + 15$  ( $d_{50} = 25 \mu\text{m}$ ), and  $-30 + 15 \mu\text{m}$  ( $d_{50} = 20 \mu\text{m}$ ), respectively. Cold spray parameters that were used here, such as the cold spray gun, deposition parameters, and feeding system, are explained in a previous work for Ni(7) and Ni(7)-WCNi coatings (Ref 19). The only distinction was the gas preheat temperature that was 800 °C for the composite coatings using Ni(25) as matrices, whereas, similar to pure Ni(7), pure Ni(25) coatings were sprayed at gas preheat temperature of 700 °C.

For each coating system, i.e., Ni and agglomerated WCNi, four steel substrates of  $3 \times 1$  inches were coated. Cold-sprayed coatings were cross sectioned perpendicular to the gun traverse direction, mechanically ground, and polished using 9-, 3-, and 1- $\mu\text{m}$  diamond pastes followed by 0.05- $\mu\text{m}$  colloidal silica. The morphology and microstructure of the initial powders and deposited coatings were observed by a scanning electron microscopy (SEM) (FEI Quanta 600, Thermo Fisher Scientific, USA). The WC and porosity concentrations within the coatings were measured by image analysis. Ten random images of polished cross sections were collected for each sample in a SEM and then analyzed by pixel count using an open-source software ImageJ. To estimate mean free path (MFP) between WCNi particles, SEM images of polished cross sections of coatings were analyzed. Random line was drawn on the images, and the number of times that the line intersects the WCNi particles was noted. The line distance was measured using the measure distance function, available in ImageJ, in which pixel counts are converted into micrometers according to the scale bar of corresponding image. Then, the number of particles intersects per unit length of the line,  $N_l$ , together with the volume fraction of WC particles,  $v_p$ , was used to estimate the MFP of the WCNi particles ( $\lambda$ ) using the following equation (Ref 26-28):

$$\lambda = \frac{1 - v_p}{N_l} \quad (\text{Eq 1})$$

At least 50 measurements were taken to obtain an average value for MFP of the WCNi particles for each coating system. Electron channeling contrast imaging (ECCI) using a cold field emission SEM (SU-8230, Hitachi, Japan), with a photodiode back-scattered electron (BSE) detector, was performed to reveal the grain and deformed structure of the coatings.

To characterize mechanical properties of Ni powder and sprayed coatings, nanohardness and microhardness testing were used. Nanohardness testing was measured using a Berkovich diamond tip with a triboindenter system (TI 950, Hysitron, USA). The peak load, loading and unloading rate, and hold time at peak load were fixed as 3 mN, 200  $\mu\text{N/s}$ , and 2 s, respectively. An array of  $10 \times 10$  was carried out on each coating system. To calculate hardness, the indentation load-displacement data during indentation were analyzed using the Oliver and Pharr method (Ref 29). The hardness of the coating is computed by the following equation (Ref 30, 31):

$$H = \frac{P_{\max}}{A} \quad (\text{Eq 2})$$

where  $P_{\max}$  is the maximum load applied and  $A$  is the projected area of indentation contact.  $A$  is dependent on the contact depth

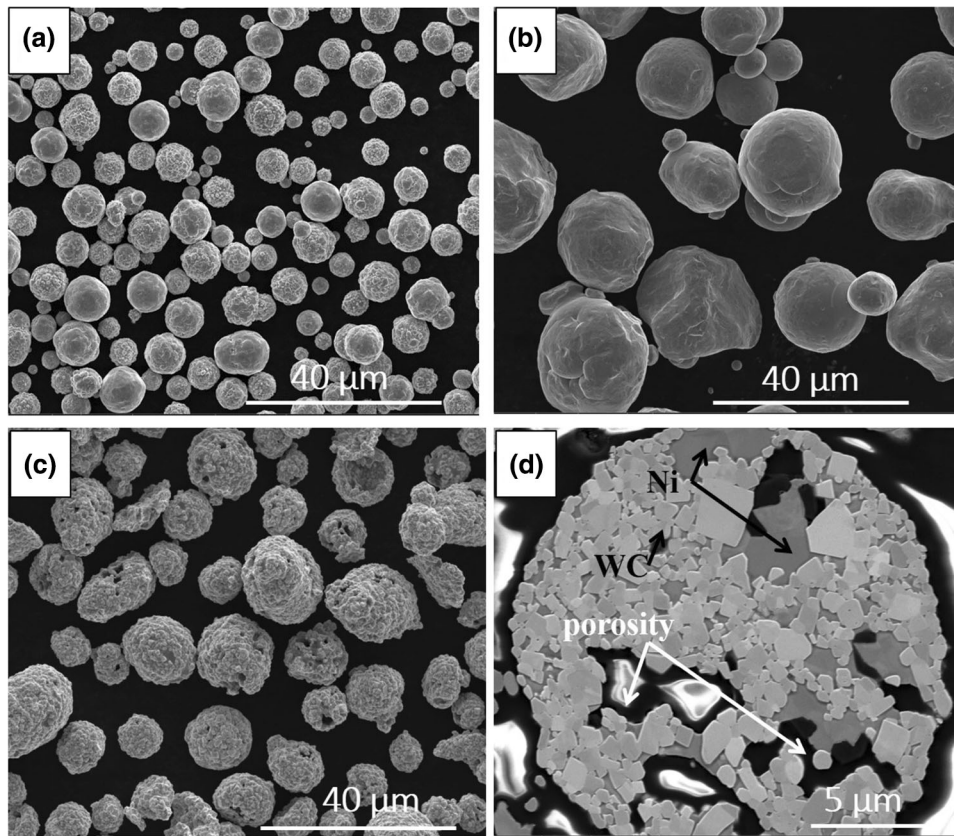


**Fig. 1** Morphology of as-received powders: (a) Ni(7) – 10 + 4 ( $d_{50} = 7 \mu\text{m}$ ), (b) Ni – 35 + 15 ( $d_{50} = 25 \mu\text{m}$ ), and (c) and (d) morphology and cross section of WCNi – 35 + 15 ( $d_{50} = 20 \mu\text{m}$ ), respectively

of the indenter according to the indenter area function (Ref 30, 31). Vickers microindentation (Clark CM-100AT, Clarke Instruments Ltd, UK) was performed on the top polished surfaces. To obtain an average hardness value of the composite, a large load of 1 kgf with a dwell time of 15 s on a microhardness tester was used. At least 20 indentations were performed on each coating system.

## 2.2 Erosion Test

SPE tests were carried out using a custom-built gas-blast erosion system based on the specifications of ASTM standard G76-13 (Ref 32, 33). Prior to erosion tests, the top surfaces of coatings were mechanically ground and polished using 9-, 3-, and 1- $\mu\text{m}$  diamond pastes followed by 0.05- $\mu\text{m}$  colloidal silica. Angular  $\text{Al}_2\text{O}_3$  particles of 20 to 70  $\mu\text{m}$  size were used as erodent particles (Fig. 2).  $\text{Al}_2\text{O}_3$  particles have an average hardness of  $13.5 \pm 0.3 \text{ GPa}$ . Back-pressure of the abrasive blasting unit was adjusted in order to control particle velocity, and its dependence on back-pressure was tested using a double-disk time-of-flight technique. A particle velocity of  $60 \pm 6 \text{ m/s}$  was obtained using 69 kPa air pressure in the nozzle. The particle feed rate was determined by altering the unit's shaker amplitude. The erosion test unit was turned on for a few minutes, while the sample was shielded by a covered shutter to stabilize the feed rate. Once feed rate was stabilized at  $0.8 \pm 0.1 \text{ g/min}$ , the test was started. The erodent powder was filled into the hopper and fed to a tungsten carbide nozzle with an inner diameter of 1.14 mm and a length of 36 mm.

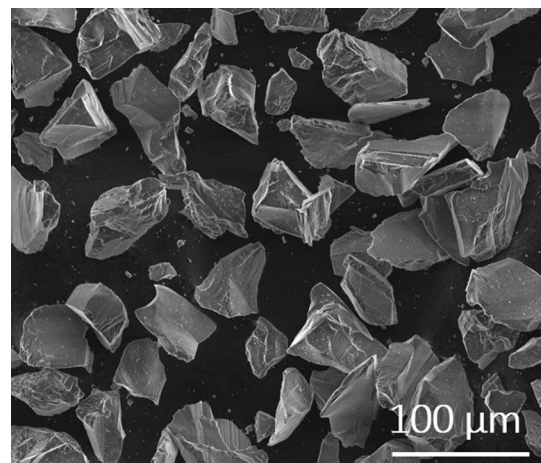


**Fig. 2** Morphology of erodent  $\text{Al}_2\text{O}_3$  particles

Working distance between the sample holder and the nozzle was kept constant at 20 mm.

The impact angle was adjusted by turning the sample holder at two different angles of impingement ( $30^\circ$  and  $90^\circ$ ). All erosion tests were performed at room temperature and 25% relative humidity. ASTM G76 standard recommends a 600-s test length (without piercing the coating) to establish the steady-state erosion rate. In this study, each test was performed for 1800 s (30 min) to better ensure steady state. At least three repetitions were made per experimental condition to evaluate

the experimental error of the measurement. Before and after the test, samples were ultrasonic cleaned in acetone and ethanol baths for 5 min, dried, and scanned using a noncontact optical profilometer (NewView 8000, Zygo Instruments, USA) to obtain profiles of the wear tracks. The erosion rate was calculated by normalizing the measured volume loss by the mass of erodent particles causing weight loss (i.e., testing time  $\times$  particle feed rate). In order to investigate erosive wear mechanisms, eroded surfaces and cross sections of wear scars were investigated using an SEM (FEI Quanta 600, Thermo Fisher Scientific, USA).

### 3. Results

#### 3.1 Coating Characterizations

Figure 3 shows micrographs of cross section and top surface of Ni coatings. Mostly spherical particles, which are likely mechanically trapped, and deformed particles were observed for cold-sprayed Ni(7) particles (Fig. 3c). However, for cold-sprayed Ni(25) particles, highly deformed and flattened particles (see Fig. 3d) were observed. Surface morphologies were consistent with internal porosity measured from cross sections, with  $1.3 \pm 0.4\%$  for Ni(25) coatings and  $3.8 \pm 0.5\%$  for Ni(7) coatings. However, Ni(7) coatings showed a higher microhardness ( $345 \pm 17$  HV<sub>1</sub>) than the Ni(25) coatings ( $215 \pm 15$  HV<sub>1</sub>), even though they were slightly more porous. Figure 4(a) and (b) shows ECC images of cross-sectioned Ni coatings. A nonuniform microstructure was observed for both coatings.

Near particle interfaces, grains are ultrafine, while the central region of the particles contains a relatively coarse structure. This was reported in previous studies and is due to an inherent feature of cold spray, where particle interfaces experience ultrahigh strains, strain rates, and adiabatic shear instability, while particle interiors experience much less deformation (Ref 34, 35). As received, both Ni powders had relatively large grain sizes of 1 to 10  $\mu\text{m}$  (not shown here). After spraying, the Ni(7) coating had cell structures with average size of 280-360 nm, which were observed near particle interfaces and are known to occur by dislocation re-arrangement (Ref 35). High strain and high strain-rate deformed microstructures are often characterized with dislocation cells, in which dislocations are trapped into low energy configuration to minimize the energy per unit length of dislocation line (Ref 36, 37). For the Ni(25) coating, cells were significantly coarser with sizes of 5-7  $\mu\text{m}$ . Nevertheless, at some interfacial regions, a fine microstructure of 300-400 nm was observed. Nanoindentation was used to measure hardness of Ni coatings. The representative load-displacement curves are given in Fig. 4(c). The average nanohardness of  $3.4 \pm 0.3$  GPa for Ni(25) coating was measured, while for Ni(7) coating it was significantly higher ( $4.8 \pm 0.7$  GPa).

Ni-WCNi composite coating properties including porosity and MFPs between WC particles are listed in Table 1. Ni(7)-WCNi coatings were slightly more porous than Ni(25)-WCNi at a given WC content in coatings. Lower MFPs between WCNi particles, as well as lower porosity, were obtained with increasing WC content in composite coatings. Figure 5 shows micrographs of cross-sectioned Ni(25)-WCNi composite coatings. Similar microstructure in terms of the WCNi splats

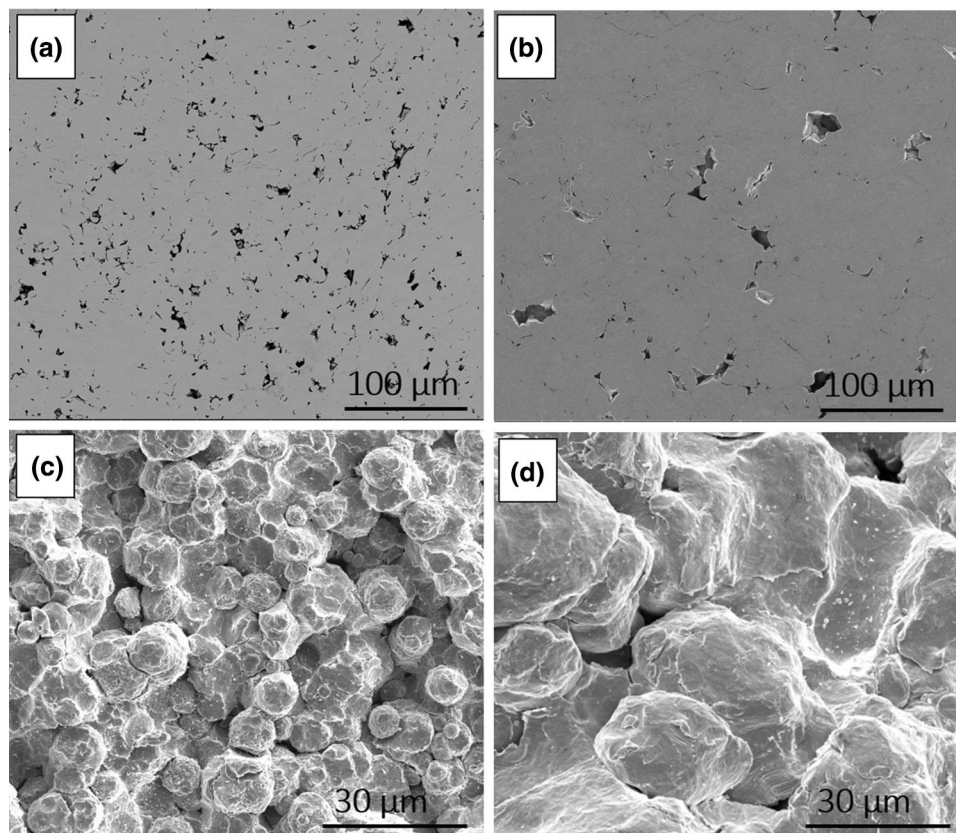


**Fig. 3** Cross-sectional morphology of (a) Ni(7), (b) Ni(25) coatings and top-down morphology of (c) Ni(7) and (d) Ni(25) coatings

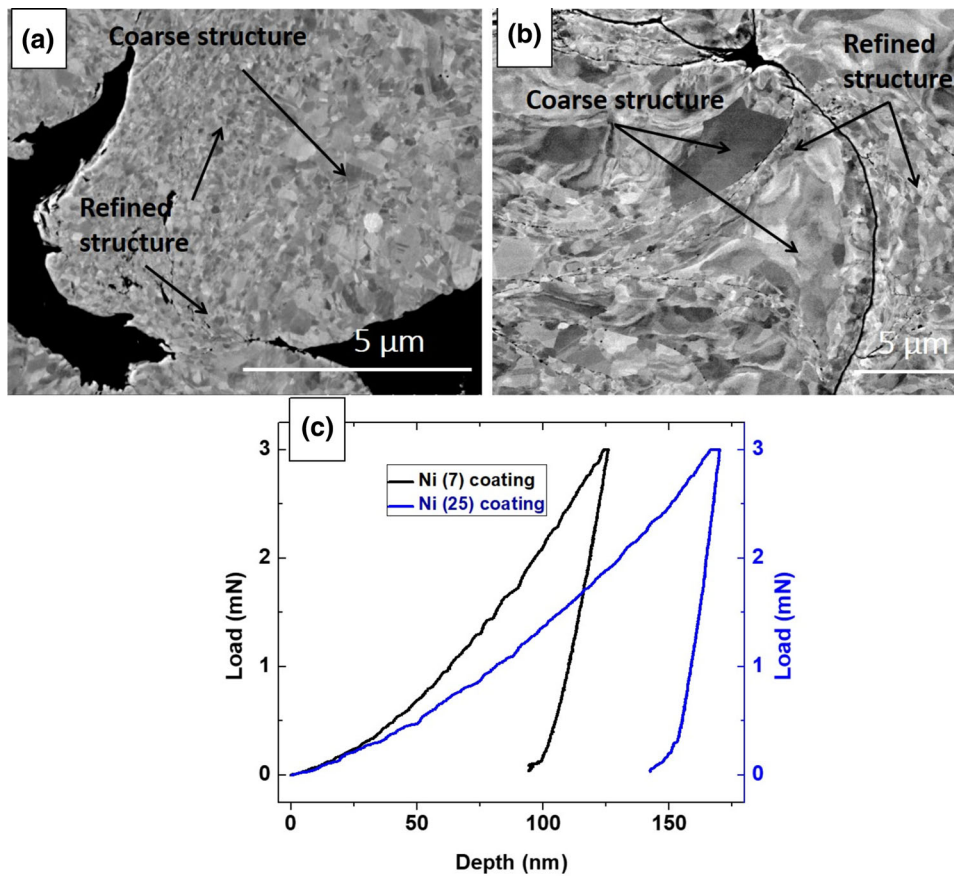


**Fig. 4** ECC imaging of (a) Ni(7) and (b) Ni(25) coatings, (c) representative load–displacement curves typically obtained from the specified coatings

**Table 1** Characteristics of cold-sprayed Ni and Ni-WC*Ni* coatings

Sample designation “Matrix-WC vol.% WC <i>Ni</i> ”	Porosity, %	MFP, μm
Ni(25)	1.3 ± 0.4	...
Ni(25)-18WCNi	1.0 ± 0.3	39 ± 4
Ni(25)-28WCNi	0.4 ± 0.2	29 ± 4
Ni(25)-39WCNi	0.4 ± 0.1	19 ± 1
Ni(25)-55WCNi	0.5 ± 0.4	15 ± 3
Ni(7)	3.8 ± 0.5	...
Ni(7)-13WCNi	1.9 ± 0.2	36 ± 5
Ni(7)-30WCNi	0.5 ± 0.2	31 ± 3
Ni(7)-43WCNi	0.4 ± 0.1	22 ± 4
Ni(7)-54WCNi	0.9 ± 0.2	18 ± 3

morphologies and MFP between WC*Ni* particles (see Table 1) was obtained for the two Ni(7)- and Ni(25)-WC*Ni* composite coatings. As can be seen in a higher-magnification view of WC*Ni* particles (Fig. 5d-f), higher compaction of WC*Ni* particles was observed in composite coatings with high WC content. With increasing WC content in coatings, porosity of coatings was decreased, except above 50 vol.% WC. Slightly higher porosity that is obtained in Ni(25)-55WCNi and Ni(7)-54WCNi coatings was due to cracking and debonding of splats (Ref 19).

Retention of WC and microhardness of coatings are shown in Fig. 6(a) and (b), respectively. WC*Ni* particles retention mechanism in Ni(7)-WC*Ni* coatings was discussed in detail in a previous work (Ref 19). Results here showed that using coarser Ni particles did not change significantly the WC recovery into coating. Retention of WC was similar when comparing Ni(7)-WC*Ni* to Ni(25)-WC*Ni* coatings (Fig. 6a). For both composite systems, WC content in coating was close to that of the initial feedstock composition, except above 60 vol.% WC in initial feedstock, in which higher retention was obtained for Ni(25)-WC*Ni* coatings. Using Ni(25) as matrix, 63 vol.% WC in feedstock powder yielded in 55 vol.% WC in coating. To obtain similar WC content in coating, a higher WC percentage, around 76 vol.%, was needed, when spraying using Ni(7).

Microhardness testing showed that incorporation of 20 vol.% WC or less into Ni did not improve the hardness of the Ni-WC*Ni* coatings compared to the pure Ni coatings. As the WC content in the coating increased further, the microhardness increased. This was related to reduced porosity and MFPs between WC*Ni* particles and increased coating density in high content WC coatings, all of which can increase the load-bearing capacity (Ref 17, 18). Moreover, higher compaction of WC*Ni* particles, which could improve adhesion between WC fragments and Ni binder, was achieved as higher WC contents were sprayed (see high-magnification images in Fig. 5). The Ni(25)-WC*Ni* showed a lower hardness when compared to Ni(7)-WC*Ni* for a given WC content in coatings, despite being

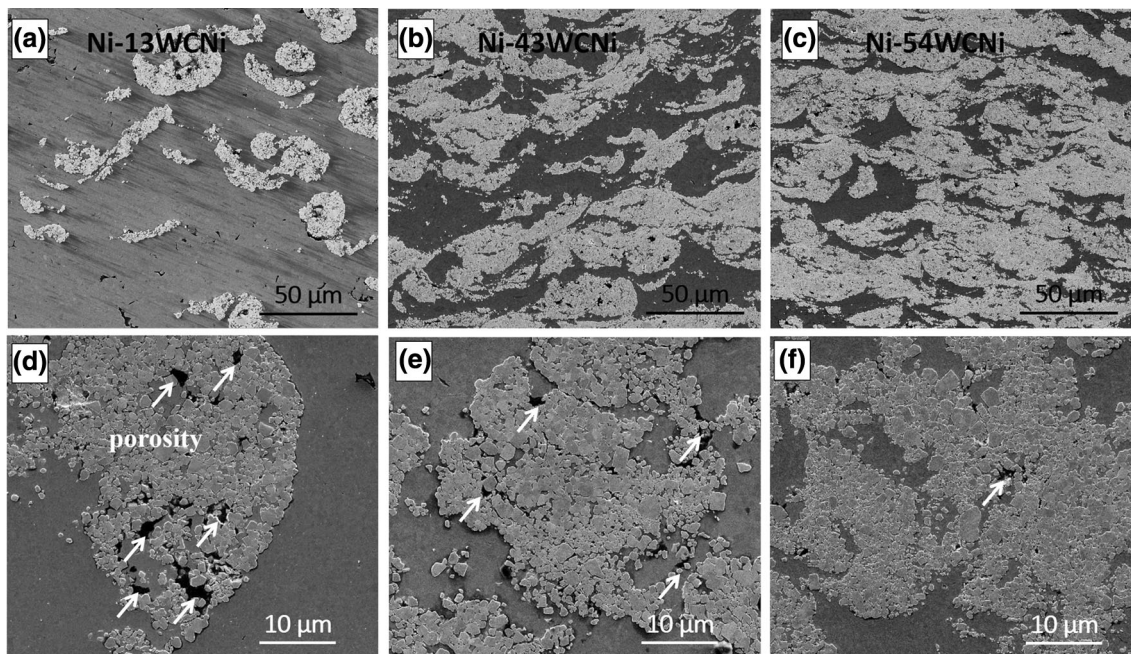


**Fig. 5** Cross-sectional morphology of (a) Ni-13WCNi, (b) Ni-43WCNi, (c) Ni-54WCNi. (d), (e), and (f) are high-magnification views of (a), (b), and (c), respectively. White arrows indicate porosities

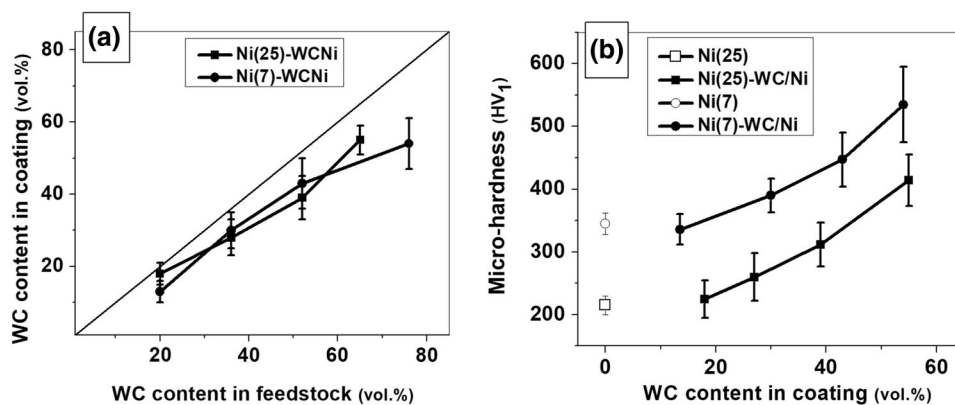


**Fig. 6** (a) WC content in the coating vs. WC content in the feedstock, (b) Vickers microhardness vs. WC content in the coating

slightly denser. The lower hardness of the Ni(25)-WCNi coatings can be attributed to the softer Ni(25) matrix.

### 3.2 SPE Testing

The volumetric erosion rates for Ni and composite coatings versus WC content in coatings are presented in Fig. 7. Erosion rates of Ni(7) were lower, as compared to Ni(25) coatings by a factor around 35 and 48% at 30° and 90° impact angles, respectively. At 30° impact angle, as shown in Fig. 7, erosion rate did not change much with incorporation of WCNi particles up to 30 vol.% WC. Erosion rates of Ni(25)-WCNi were higher than those recorded for Ni(7)-WCNi at a given WC content in coatings. Addition of around 40 and 55 vol.% in Ni(7) and 55 vol.% in Ni(25) led to a significant drop (80-85%) in erosion rates, where the erosion rates of the two composite systems approached around the same values. Under normal impacts, addition of WCNi into Ni(25) was found to slightly decrease the erosion damage, only around 20%, and it was independent of WC content. For Ni(7)-WCNi coatings, no notable change of

erosion rates at normal impact was detected by incorporation of the hard phase.

For both Ni coatings, the erosion rate at 30° was higher than that at 90°, indicating ductile erosion, in which materials removal predominantly takes place by plastic deformation (i.e., cutting, plowing). Similar characteristics of ductile erosion were recorded for Ni-WCNi composite coatings up to 30 vol.% WC, while for Ni-WCNi composite coatings with WC content of 40 and 55 vol.%, erosion rates at 90° were slightly higher than that at 30°. This indicates a transition in erosion mechanism from ductile to brittle behavior (Ref 3, 4) and will be discussed in more details in section 4.

### 3.3 Analysis of the Worn Surface and Subsurface

**3.3.1 Pure Ni Coatings.** SPE behavior of Ni(7) was reported in an earlier work (Ref 25). In this study, SPE of Ni(25) was compared to that of Ni(7). Micrographs of Ni worn surfaces are presented in Fig. 8, for both impact angles. For

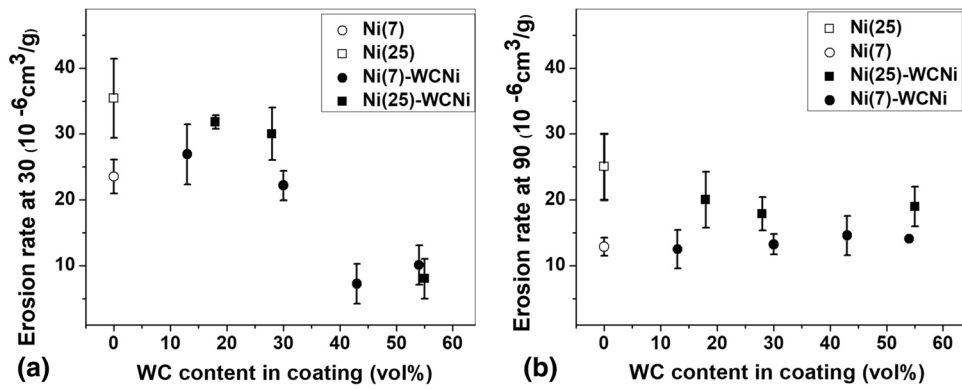


**Fig. 7** Variation of erosion rate with WC vol.% tested at (a) 30° and (b) 90° impact angle. Scatter bars indicate the standard deviation of 6 repeat measurements

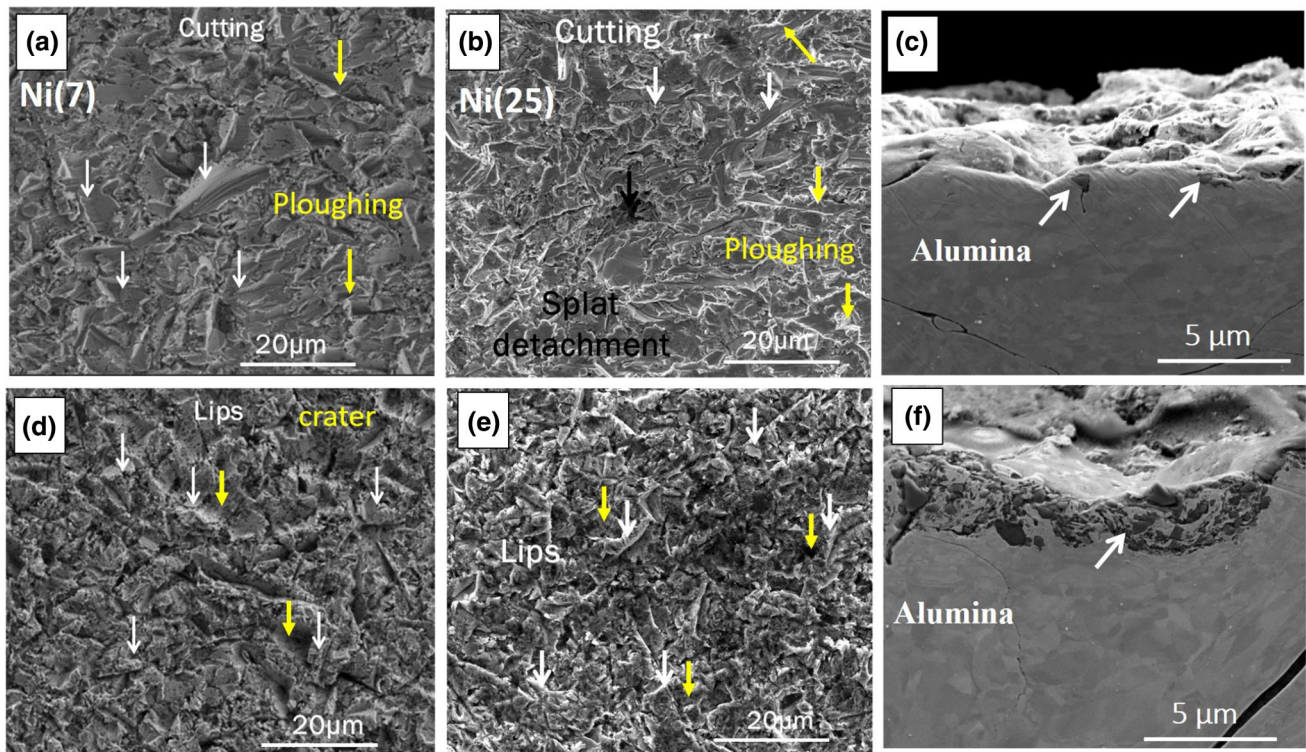


**Fig. 8** SEM micrographs of worn surfaces of (a) Ni(7), (b) Ni(25), and (c) subsurface of worn Ni(25) coatings after 30-min erosion test at 30° impact angle, worn surfaces of (d) Ni(7), (e) Ni(25), and (f) subsurface of worn Ni(25) coatings after 30-min erosion test at 90° impact angle. For 30° impact angle, impact direction was from left to right. For 90° impact angle, impact direction was normal to the plane

both coatings, at 30°, worn surface morphologies exhibited materials removal by cutting and plowing (Fig. 8a and b). At normal impacts, features associated with crater and lip formations were observed on the worn surfaces (Fig. 8d and e). Similar results were reported in previous studies on SPE of metallic materials, where the material removal is mainly due to the microcutting and plowing action of the erodent particle at low impact angle, whereas lip formation, strain hardening of lips, and subsequent cutting/fracture of these lips in the form of thin platelets are active material removal modes under normal impact (Ref 38, 39).

Analysis of subsurface microstructure of Ni(7) in a previous work (Ref 25) revealed embedding of erodent particles into Ni worn surfaces, which was more frequently

observed on 90° impact angle, as compared to 30°, and caused a shielding effect against severe erosion loss. More severe wear for Ni(25) was consistent with higher erosion rate, at some regions where deep craters were formed. Subsurface analysis of Ni(25) (Fig. 8c and f) revealed embedding of  $\text{Al}_2\text{O}_3$  particles, more frequently observed under 90° angle of incidence, similar to Ni(7) coatings. The features on the worn surfaces for both coatings implied typical damage of ductile erosion, which is consistent with the angular dependence of erosion rates.

**3.3.2 Ni-WC Ni Composite Coatings.** To investigate the surface damage on the composite coatings due to  $\text{Al}_2\text{O}_3$  particle erosion, worn surfaces were analyzed by SEM. Cutting and

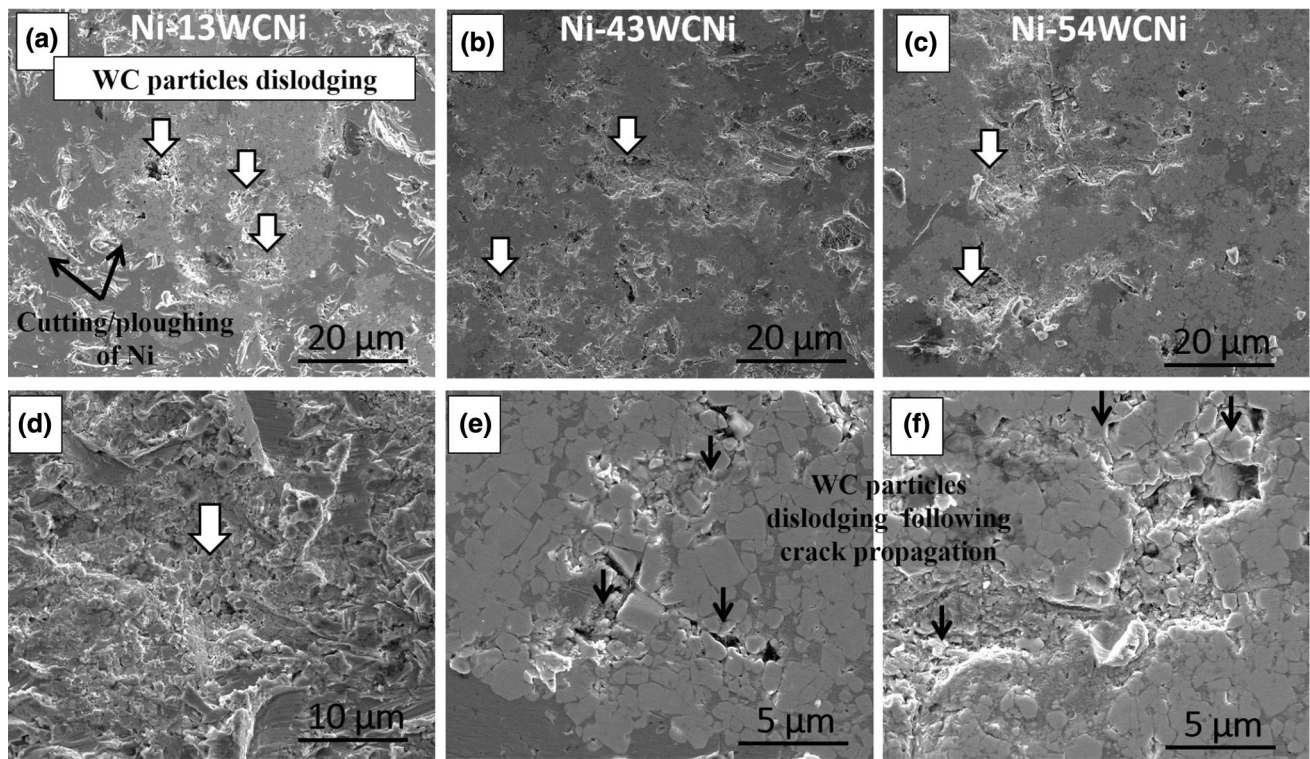


**Fig. 9** SEM micrographs of worn surfaces of (a) Ni(7)-13WCNi, (b) Ni(7)-43WCNi, and (c) Ni(7)-54WCNi coatings after 30-min erosion test at 30° impact angle. (d), (e), and (f) are high-magnification views of (a), (b), and (c), respectively. Impact direction was from left to right

plowing of Ni matrices was observed that was similar to erosion of pure Ni coatings. From worn surface morphologies that were obtained on the central regions of wear scar, it is difficult to determine the prevailing mechanism due to substantial number of impact events and combined mode of erosion mechanism. Therefore, the “halo” regions on worn surfaces, where there were only a few impact events, were analyzed. Figure 9 shows the surface morphology in the halo regions of wear scars for Ni(7)-WCNi coatings at 30° impact angle. It is evident that Ni was preferentially worn away. The WCNi particles were also eroded; however, the type of damage was found to shift from knocking out of WC fragments from the surface at low content WC to combined dislodgment and microcracking of WC fragments for high WC content composites (Fig. 9). Similar shift in erosion mechanism was observed for WCNi particles in Ni(25)-WCNi coatings (not shown here). This implies that densification and improved adhesion between WC fragments/Ni binder may contribute to improved erosion resistance, in addition to WC incorporation itself. Figure 10 shows the surface morphology on the halo regions of the wear scars for Ni(7)-WCNi coatings at 90° impact angles. Lips formation for Ni matrices was observed. At low WC concentrations, WCNi particles behaved ductile, as evidenced by the indentation marks of erodent particles with no sign of cracking on the worn surfaces. However, cracking of WC particles was recorded with increasing WC contents in coatings (Fig. 10). Similar observations were made for WCNi particles in Ni(25)-WCNi coatings under normal impacts.

Another interesting observation was the presence of a few deep and large craters (Fig. 11a and c) for the highest WC content coatings, both Ni(7)-54WCNi and Ni(25)-55WCNi, detected at both angles. Subsurface images of Ni(7)-54WCNi

worn surfaces revealed crack propagation along WCNi boundaries (Fig. 11d and f). The removal of large patches of materials, following subsurface crack propagation, can be related to the slight increase in erosion rates at both angles, when compared to Ni-40WCNi.

## 4. Discussion

### 4.1 Cold Spray Deposition of Ni and Ni-WC Ni Coatings

Ni-WC Ni coatings were cold sprayed using two different size distributions of Ni powders and varying amounts of WCNi in the feedstock. The WCNi particles retention and their distribution and morphologies were not influenced by the size of Ni powders. However, properties of the coatings did change with WC content and also with the size of Ni powder used. The expected trend of increased hardness with increasing WCNi was observed. This was due to the fact that WCNi particles were more densified upon impact, suggesting an improvement in adhesion of these particles. Lower MFPs between WCNi particles and improved adhesion between WC and Ni binder would naturally enhance hardness of coatings with high WC content.

The effect of the size of the Ni powder in the feedstock on the coating properties requires exploration of the coating microstructure, which was also discussed in detail in a previous work (Ref 19). Comparing Ni(7) and Ni(25) particles, Ni(25) particles underwent more severe plastic deformation compared to Ni(7) particles during spraying. Previous studies showed that shear instability in smaller metallic particles can be hindered because of higher cooling rates during impact and intensified



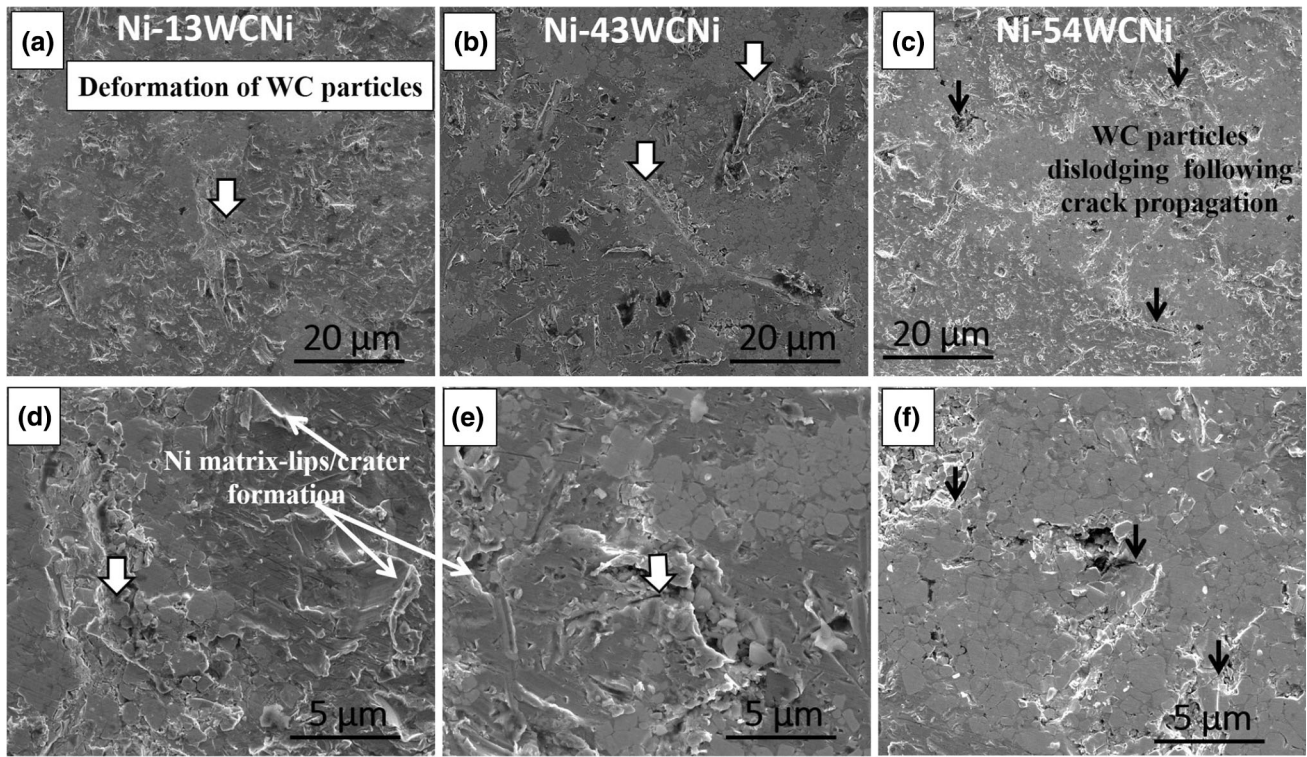


**Fig. 10** SEM micrographs of worn surfaces of (a) Ni(7)-13WCNi, (b) Ni(7)-43WCNi, and (c) Ni(7)-54WCNi coatings after 30-min erosion tested at 90° impact angle. (d), (e), and (f) are high-magnification views of (a), (b), and (c), respectively. Impact direction was normal to the plane

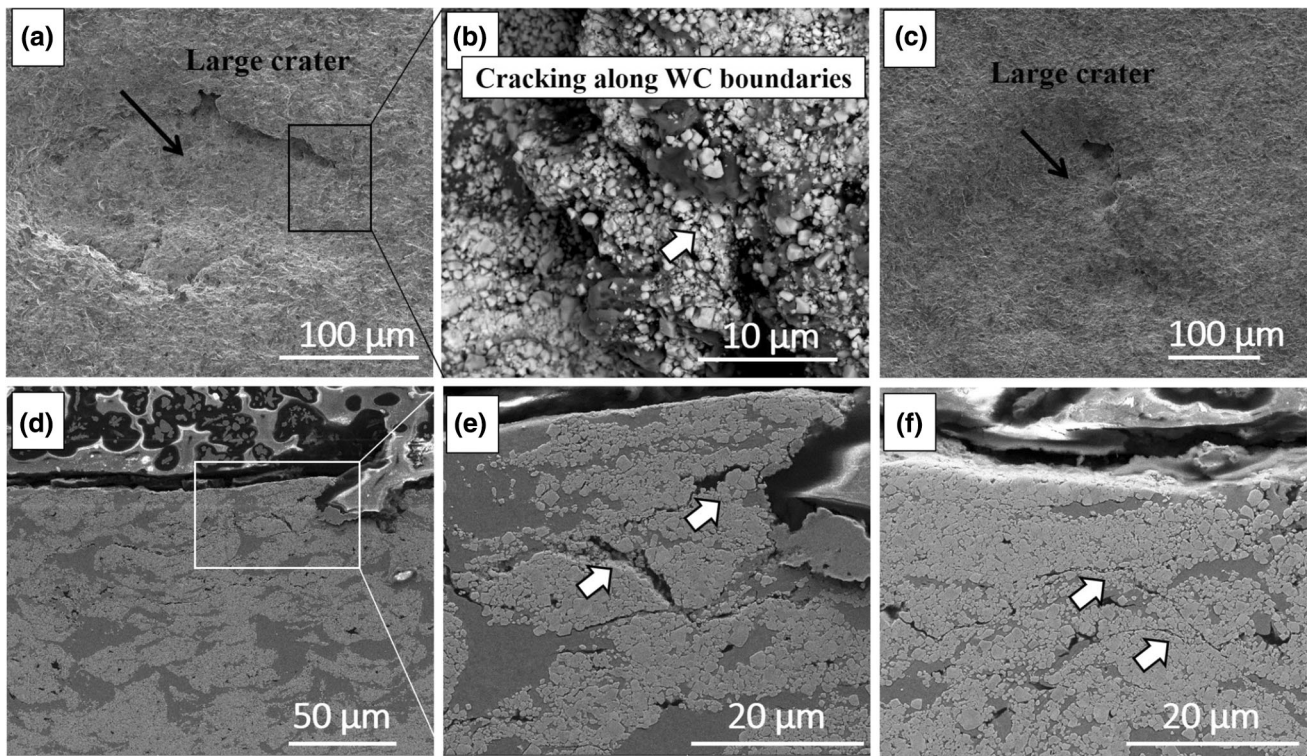


**Fig. 11** SEM micrographs of worn surfaces of (a) Ni(7)-54WCNi, (c) Ni(25)-55WCNi, after 30-min erosion tested at 30° impact angle, (b) BSE high-magnification view of (a). Subsurface microstructure of Ni(7)-54WCNi tested at (d) 30°, (f) 90° impact angles. (e) High-magnification view of (d). For 30° impact angle, impact direction was from left to right

strain-rate hardening (Ref 40). Ni(25) coating featured a coarser microstructure compared to Ni(7) coating. This may be explained by a higher driving energy for restoration mechanisms in highly deformed Ni(25) particles during cold spraying, where the initial increase in dislocation density at some regions is dynamically restored. Whereas, for finer size Ni(7), the extent of plastic deformation is significantly lower, thus, there is insufficient energy to activate restoration mechanisms. Another possible reason can be the lower dissipation rate of gas heat transferred to Ni(25) particles during cold spraying, which means the deposited particles spend more time at higher temperature and can undergo restoration more readily. Micro- and nanohardness testing showed Ni(25) coatings were softer than Ni(7) coatings, due to coarser microstructure, despite being slightly less porous. In coarser cells of Ni(25) coatings, there is less hindrance to the dislocation movement, thus resulting in lower resistance to plastic deformation and lower hardness when compared to finer microstructure in Ni(7) coatings. Addition of WCNi particles to Ni matrix densified the coatings for both composite systems; however, it did not influence microstructure of Ni matrices. Nanohardness testing on Ni matrices of composite coatings showed similar values that were obtained for pure Ni coatings. On a larger scale indentation, microhardness of composite coatings with WC content above 20 vol.% was higher than that of pure Ni coatings. Ni(7) and Ni(7)-WCNi coatings were harder than Ni(25) and Ni(25)-WCNi coatings at a given WC content in coating, due to more refined matrix microstructure.

#### 4.2 SPE Behavior of Ni and Ni-WC Ni Coatings

Ni and Ni-WC Ni coatings were subjected to SPE tests. It was found that Ni(7) coatings were more wear resistant when compared to Ni(25) coatings, under both impact angles. Examination of cross sections and surfaces of eroded Ni coatings suggested that the erosion occurs through ductile mechanisms. Higher resistance to plastic deformation and cutting action of erodent particles in Ni(7) coatings, due to their higher hardness when compared to Ni(25), led to lower erosion rates. The similar mechanisms were maintained for Ni matrices in Ni-WC Ni composite coatings. In fact, no considerable influence on Ni matrices erosion was recorded when WC was added. This could be due to weak bonding between Ni and WC Ni particles in cold-sprayed coatings, where WC Ni bonded to matrix by mechanical interlocking. Another crucial factor that must be considered is the homogeneity of the material with respect to the contact area of the abrasive particles. In erosive wear, the influence of the reinforcement contents is highly dependent on the wear conditions. The “scale of individual contacts” (Ref 3) has a key effect on the erosion behavior of MMCs. A large contact area of the abrasive particles compared to the scale of the material microstructure defines material as homogeneous and vice versa, and small contact area of the erodent particles when compared to the scale of microstructure leads to inhomogeneous wear behavior of the material (Ref 3). Previous studies reported that when a heterogeneous composite is subjected to wear, the binder phase will preferentially wear, and eventually the hard particles will fall out of the matrix, unless strong bonding between matrix and reinforcement particles prevents reinforcement dislodging too easily from the matrix (Ref 8, 9, 11-13, 41). In this study, the erodent particles were angular with the size from 20 to 70  $\mu\text{m}$ ; however, sharp grooving edges of the particles are much

smaller. SPE of Ni-WC Ni composite coating can be defined as heterogeneous, when the “scale of individual contacts” is concerned, i.e., smaller contact area than microstructure scales of the composite coatings, MFPS between WC Ni particles in the present case. Considering the scale effect, the erosion performance of the coatings can depend mainly on one of the three factors: matrix, WC Ni reinforcements, or WC Ni/Ni interfaces, i.e., which one is the “weakest link” in the structure concerning wear. Likewise, erosion of reinforcements, WC Ni particles, is controlled by adhesion of WC fragments to Ni binder.

At 30° impact angle, erosion rate measurements showed that up to 30 vol.% WC additions to Ni did not influence its wear performance. This is due to weak mechanical bonding of WC Ni particles to Ni matrices as well as porosities which remained inside WC Ni particles at low content WC coatings. A high concentration of WC of above 40 vol.% was needed for a drop in erosion rates for both composite systems assisted by a mechanism change from ductile erosion of matrix and knocking out of WC fragments to intergranular crack propagation. This is supported by surface and subsurface observations (see Fig. 11), where crack propagation along WC Ni boundaries caused deep and large craters. At high content WC coatings, linking between WC particles prevents crack arresting by Ni plastic deformation. Therefore, plastic strain accumulated in WC caused crack propagation along WC Ni boundaries. A significant volume of material was detached from the surface when cracks intersected. Erosion rates of Ni(7)-40 and 55WC Ni coatings were close to that measured for Ni(25)-55WC Ni, despite different Ni matrices, which supports the view that erosion rate was controlled by the subsurface cracking of WC Ni particles network.

Under normal impact angle, incorporation of WC Ni particles slightly decreased erosion rate at low concentration of agglomerated WC Ni particles. When subjected to erosive wear, compaction and deformation of WC Ni particles near the contact area occurred through slipping and rotation of WC particles along the Ni binder. This is because voids were present between WC particles, along with porosity inside the powders and Ni binder between WC agglomerates, which provide ductility. However, a high degree of compaction, achieved in high concentration of agglomerated WC Ni particles, caused crack propagation due to strain accumulation.

## 5. Conclusion

Two size ranges of Ni,  $-10 + 4$  ( $d_{50} = 7 \mu\text{m}$ ) and  $-35 + 15$  ( $d_{50} = 25 \mu\text{m}$ ), were sprayed alone and mixed with WC Ni powders. Solid particle erosion wear performance of Ni and Ni-WC Ni composite coatings was studied. Ni(7) coatings were harder and more erosion resistant than Ni(25) coatings. The size of Ni particles did not change the WC retention to coating, and the concentration of WC in sprayed Ni-WC Ni coatings was similar and close to that of the initial feedstock for both Ni powders. It was found that Ni-WC Ni coatings can be tailored to contain 13-55 vol.% WC and display a varied hardness ranging between 225 and 550 HV<sub>1</sub>. Higher concentration of WC Ni in initial feedstock led to more compaction of WC Ni particles in the coatings. At low WC contents in the coating, erosion performance was controlled by Ni matrices and WC knocking out from the surface, whereas a higher concen-

tration of WC/Ni particles increased erosion resistance for low angles, due to improved resistance to dislodging and improved adhesion between Ni binder and WC fragments. For the highest WC concentration coatings, due to linking between WC particles, the crack propagation was not arrested by Ni deformation, which led to slight increase in erosion rate. The lowest erosion rate was identified in the coating that featured 40 vol.% of WC in a fine Ni(7) matrix.

## Acknowledgments

The authors gratefully acknowledge the financial support from the Canadian Foundation for Innovation (CFI) Project No. 8246 for the cold spray equipment, the CFI Leader's Opportunity Fund Project No. 13029 for the tribometer and nanoindentation equipment, and the Natural Sciences and Engineering Research Council (NSERC) Strategic Grants Program for the operational funding of this project. Thanks are also due to Tekna Inc. for providing the Ni and spherical WC powders. The authors acknowledge administrative support from Drs. Phuong Vo, Eric Irissou, and Jean-Gabriel Legoux and technical support from Mr. Jean Francois Alarie at the McGill Aerospace Materials and Alloy Design Center (MA-MADC) cold spray facility at NRC-Boucherville. The authors thank the Functional Coatings and Surface Engineering Laboratory (FCSEL) at Polytechnique Montréal and greatly acknowledge the assistance of Dr. Etienne Bousser with the erosive wear testing and analysis.

## References

- W. Thorn, J. Schell, M.L. Lasonde, G. Hein, M. Klein, and M. Mendez, *Erosion Durability Improvement of the T64 Engine for Military Helicopters*. Paper Presented at the American Helicopter Society 60th Annual Forum Baltimore, MDed., 2004
- ASM handbook. *Volume 18, Friction, Lubrication, and Wear Technology*, 1992
- I. Hutchings and P. Shipway, *Tribology Friction and Wear of Engineering Materials*, 2nd ed., Butterworth-Heinemann, Oxford, 1992
- I. Finnie, Some Reflections on the Past and Future of Erosion, *Wear*, 1995, **186**(1), p 1–10
- J.M. Miguel, J.M. Guilemany, and S. Vizcaino, Tribological Study of NiCrBSi Coating Obtained by Different Processes, *Tribol. Int.*, 2003, **36**(3), p 181–187
- P.L. Hurricks, Some Aspects of Metallurgy and Wear Resistance of Surface Coatings, *Wear*, 1972, **22**(3), p 291–320
- P. Kulu, Erosion Resistance of Powder Materials and Coatings, *J. Tribol.*, 1989, **8**(4), p 12–25
- C.P. Paul, S.K. Mishra, P. Tiwari, and L.M. Kukreja, Solid-Particle Erosion Behaviour of WC/Ni Composite Clad Layers with Different Contents of WC Particles, *Opt. Laser Technol.*, 2013, **50**, p 155–162
- P. Kulu and T. Pihl, Selection Criteria for Wear Resistant Powder Coatings Under Extreme Erosive Wear Conditions, *J. Therm. Spray Technol.*, 2002, **11**(4), p 517–522
- M.R. Ramesh, S. Prakash, S.K. Nath, P.K. Sapra, and B. Venkataraman, Solid Particle Erosion of HVOF Sprayed WC-Co/NiCrFeSiB Coatings, *Wear*, 2010, **269**, p 197–205
- M.G. Gee, C. Phatak, and R. Darling, Determination of Wear Mechanisms by Stepwise Erosion and Stereological Analysis, *Wear*, 2005, **258**(1–4), p 412–425
- I. Hussainova, M. Antonov, and A. Zikin, Erosive Wear of Advanced Composites Based on WC, *Tribol. Int.*, 2012, **46**(1), p 254–260
- R. Zhou, Y.H. Jiang, and D.H. Lu, The Effect of Volume Fraction of WC Particles on Erosion Resistance of WC Reinforced Iron Matrix Surface Composites, *Wear*, 2003, **255**, p 134–138
- V.K. Champagne, *The Cold Spray Materials Deposition Process: Fundamentals and Applications*, Woodhead/CRC Press, Cambridge/Boca Raton, 2007
- G.-C. Ji, H.-T. Wang, X. Chen, X.-B. Bai, Z.-X. Dong, and F.-G. Yang, Characterization of Cold-Sprayed Multimodal WC-12Co Coating, *Surf. Coat. Technol.*, 2013, **235**, p 536–543
- H.-T. Wang, X. Chen, X.-B. Bai, G.-C. Ji, Z.-X. Dong, and D.-L. Yi, Microstructure and Properties of Cold Sprayed Multimodal WC-17Co Deposits, *Int. J. Refract. Metal Hard Mater.*, 2014, **45**, p 196–203
- N.M. Melendez and A.G. McDonald, Development of WC-Based Metal Matrix Composite Coatings Using Low-Pressure Cold Gas Dynamic Spraying, *Surf. Coat. Technol.*, 2013, **214**, p 101–109
- D. Lioma, N. Sacks, and I. Botef, Cold Gas Dynamic Spraying of WC-Ni Cemented Carbide Coatings, *Int. J. Refract. Met. Hard*, 2015, **49**, p 365–373
- S.A. Alidokht, P. Vo, S. Yue, and R.R. Chromik, Cold Spray Deposition of Ni and WC-Reinforced Ni Matrix Composite Coatings, *J. Therm. Spray Technol.*, 2017, **26**(8), p 1908–1921
- M. Couto, S. Dosta, M. Torrell, J. Fernandez, and J.M. Guilemany, Cold Spray Deposition of WC-17 and 12Co Cermets Onto Aluminum, *Surf. Coat. Technol.*, 2013, **235**, p 54–61
- H.J. Kim, C.H. Lee, and S.Y. Hwang, Fabrication of WC-Co Coatings by Cold Spray Deposition, *Surf. Coat. Technol.*, 2005, **191**(2–3), p 335–340
- C.J. Li, G.J. Yang, P.H. Gao, J. Ma, Y.Y. Wang, and C.X. Li, Characterization of Nanostructured WC-Co Deposited by Cold Spraying, *J. Therm. Spray Technol.*, 2007, **16**(5–6), p 1011–1020
- P.H. Gao, Y.G. Li, C.J. Li, G.J. Yang, and C.X. Li, Influence of Powder Porous Structure on the Deposition Behavior of Cold-Sprayed WC-12Co Coatings, *J. Therm. Spray Technol.*, 2008, **17**(5–6), p 742–749
- T. Peat, A. Galloway, A. Toumpis, P. McNutt, and N. Iqbal, The Erosion Performance of Cold Spray Deposited Metal Matrix Composite Coatings with Subsequent Friction Stir Processing, *Appl. Surf. Sci.*, 2017, **396**, p 1635–1648
- S.A. Alidokht, P. Vo, S. Yue, and R.R. Chromik, Erosive Wear Behavior of Cold-Sprayed Ni-WC Composite Coating, *Wear*, 2017, **376**, p 566–577
- N.M. Melendez, V.V. Narulkar, G.A. Fisher, and A.G. McDonald, Effect of Reinforcing Particles on the Wear Rate of Low-Pressure Cold-Sprayed WC-Based MMC Coatings, *Wear*, 2013, **306**(1–2), p 185–195
- M. Kouzeli and A. Mortensen, Size Dependent Strengthening in Particle Reinforced Aluminium, *Acta Mater.*, 2002, **50**(1), p 39–51
- P. Chivavibul, M. Watanabe, S. Kuroda, J. Kawakita, M. Komatsu, K. Sato, and J. Kitamura, Effect of Powder Characteristics on Properties of Warm-Sprayed WC-Co Coatings, *J. Therm. Spray Technol.*, 2010, **19**(1–2), p 81–88
- W.C. Oliver and G.M. Pharr, An Improved Technique for Determining Hardness and Elastic-Modulus Using Load and Displacement Sensing Indentation Experiments, *J. Mater. Res.*, 1992, **7**(6), p 1564–1583
- A.C. Fischer-Cripps, *Nanoindentation, Mechanical Engineering Series*, Springer, Berlin, 2002
- Hysitron, *TI, 950 Triboindenter User Manual Revision 9.3.0314*, Hysitron Incorporated, Billerica, 2014, p 1–256
- ASTM-G76, *Standard Test Method for Conducting Erosion Tests by Solid Particle Impingement Using Gas Jets*, West Conshohocken, PA, 2007, p 1–6
- E. Bousser, L. Martinu, and J.E. Klemberg-Sapieha, Solid Particle Erosion Mechanisms of Protective Coatings for Aerospace Applications, *Surf. Coat. Technol.*, 2014, **257**, p 165–181
- Y. Zou, D. Goldbaum, J.A. Szpunar, and S. Yue, Microstructure and Nanohardness of Cold-Sprayed Coatings: Electron Backscattered Diffraction and Nanoindentation Studies, *Scripta Mater.*, 2010, **62**(6), p 395–398
- C. Borchers, F. Gartner, T. Stoltenhoff, H. Assadi, and H. Kreye, Microstructural and Macroscopic Properties of Cold Sprayed Copper Coatings, *J. Appl. Phys.*, 2003, **93**(12), p 10064–10070
- L.E. Murr, C.S. Niou, S. Pappu, J.M. Rivas, and S.A. Quinones, Leds in Ultra-High Strain-Rate Deformation, *Phys. Status Solidi A*, 1995, **149**(1), p 253–274
- B. Bay, N. Hansen, D.A. Hughes, and D. Kuhlmann-Wilsdorf, Overview No. 96 Evolution of f.c.c. Deformation Structures in Polyslip, *Acta Metall. Mater.*, 1992, **40**(2), p 205–219

38. A.S. Praveen, J. Sarangan, S. Suresh, and J.S. Subramanian, Erosion Wear Behaviour of Plasma Sprayed NiCrSiB/Al<sub>2</sub>O<sub>3</sub> Composite Coating, *Int. J. Refract. Met. Hard.*, 2015, **52**, p 209–218
39. Z. Hongwei, D. Xiaohui, and C. Shuguang, Solid Particle Erosion-Wear Behaviour of Cr<sub>3</sub>C<sub>2</sub>-NiCr Coating on Ni-Based Superalloy, *Adv. Mech. Eng.*, 2017, **9**(3), p 1–9
40. T. Schmidt, F. Gärtner, H. Assadi, and H. Kreye, Development of a Generalized Parameter Window for Cold Spray Deposition, *Acta Mater.*, 2006, **54**(3), p 729–742
41. H. Wang, W.M. Xia, and Y.S. Jin, A Study on Abrasive Resistance of Ni-Based Coatings with a WC Hard Phase, *Wear*, 1996, **195**(1-2), p 47–52

**Publisher's Note** Springer Nature remains neutral with regard to jurisdictional claims in published maps and institutional affiliations.